Chinese Chemical Letters 34 (2023) 108019

Contents lists available at ScienceDirect

Chinese Chemical Letters

journal homepage: www.elsevier.com/locate/cclet

Conjugation expansion strategy enables highly stable all-polymer solar cells

Dingding Qiu[a,b,d], Yanan Shi[a,b], Yi Li[a,c], Jianqi Zhang[a], Kun Lu[a,b,*], Zhixiang Wei[a,b]

[a] CAS Key Laboratory of Nanosystem and Hierarchical Fabrication, CAS Center for Excellence in Nanoscience, National Center for Nanoscience and Technology, Beijing 100190, China
[b] University of Chinese Academy of Sciences, Beijing 100049, China
[c] Department of Chemistry, Molecular Dynamic Chemistry Center, Tianjin Key Laboratory of Molecular Optoelectronic Sciences, School of Science, Tianjin University, Tianjin 300354, China
[d] Sino-Danish Center for Education and Research, Sino-Danish College, University of Chinese Academy of Sciences, Beijing 100049, China

ARTICLE INFO

Article history:
Received 25 September 2022
Revised 15 October 2022
Accepted 22 November 2022
Available online 25 November 2022

Keywords:
Polymer donor
Conjugation expansion
All-polymer organic solar cells
Stability
Crystallinity

ABSTRACT

The stability issue is one of the key factors hindering the commercial application of organic solar cells. All-polymer organic solar cell is one of the effective ways to solve the stability problem. In this work, we designed and synthesized two polymer donor materials PBDT and PDTBDT with different conjugation ranges, and demonstrated for the first time that extending the conjugation range of donor materials in all polymer solar cells can significantly improve device efficiency and stability. The experimental results of materials and devices show that PDTBDT with a larger conjugation range has stronger crystallinity and a more planar structure, which endows the active layer in its corresponding device with higher exciton dissociation probability, lower carrier recombination probability, more balanced charge transport properties and more favorable film morphology. As a result, the PDTBDT:PYF-T-*o* devices display an outstanding PCE of 13.38%, which is much higher than PBDT with smaller conjugation range based devices. Moreover, the PDTBDT:PYF-T-*o* device retains 0.86 of the initial PCE after over 500 h in the air atmosphere, exhibiting significantly improved stability. The improved stability is attributed to the enhanced moisture and air tolerance of active layer film thanks to the strong crystallinity of the donor material. These results demonstrate that the conjugation expansion strategy is one of the effective ways to obtain efficient and stable all-polymer organic solar cells.

Organic solar cells (OSCs), employing organic donor and acceptor materials as the photoactive layer, is one of the most promising photovoltaic technology for industrialization because of their unique advantages of light weight, mechanical flexibility and low-cost fabrication by solution processing [1–3]. Over the past several years, the power conversion efficiency (PCE) of OSCs have increased rapidly to over 20%, benefiting from progresses in design and synthesis of novel materials, device preparation methods, physical operating mechanism and so on [4–8]. Inevitably, the stability problem has become one of the most important factors hindering industrialization and has attracted more and more attentions of researchers [9–11]. As a significant and effective workaround for this issue, all-polymer solar cells (all-PSCs) presented enhanced devices stability under different external conditions, demonstrating that all-PSCs is prospective to deliver superior devices performances in practical applications comparing with their small molecular counterparts [12–14]. Superior long-term stability of all-PSCs is mainly from the intrinsic long continuous molecular chains structure of polymer acceptors, which endows all-PSCs outstanding mechanical, thermal and storage stability [15,16]. These properties of all-PSCs make them more suitable for roll-to-roll processing in industrial production.

During the evolution of all-PSCs, the development of polymer donor and acceptor materials played a critical role [17–19]. In the past few years, the continuous innovation of polymer acceptor materials has driven the continuous improvement of PCEs of all-PSCs [20–23]. However, the donor materials involved were always limited to several ones, such as PBDB-T, PM6 and PTzBI-*o*F [24,25]. And these materials often deliver inferior performances in all-PSCs than in polymer-small molecular OSCs. Therefore, exploring novel polymer donor materials favorably matching polymer acceptors es-

* Corresponding author.
E-mail address: lvk@nanoctr.cn (K. Lu).

https://doi.org/10.1016/j.cclet.2022.108019
1001-8417/

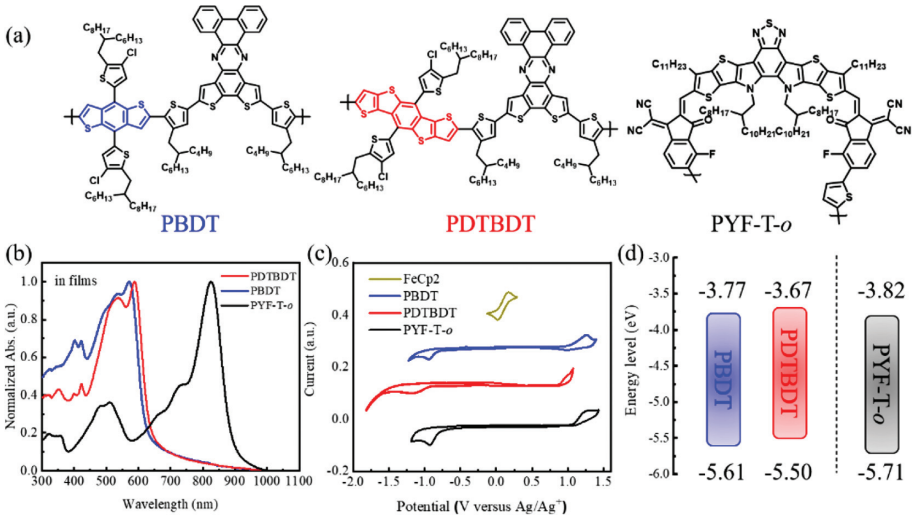

Fig. 1. (a) Chemical structures, (b) absorption spectra in thin films, (c) cyclic voltammograms, and (d) energy levels of PBDT, PDTBDT and PYF-T-*o*.

pecially polymerized Y6 derivatives, is an essential and hopeful striving direction for all-PSCs with excellent performance and stability.

Among the rational molecular design principles, conjugation expansion strategy is valid and considerable, for the significant influence of conjugation range of polymer donors on material crystallinity and absorption, photoactive layer morphology and device performances [26–30]. Extending the conjugation range of polymer donors tends to promote electron delocalization, which in turn greatly affects molecular conformation, the disorder of the molecular skeleton and the rigidity of the molecular [31]. This strategy has been proven to be effective in designing efficient polymer and small molecule donor materials. Tang *et al.* constructed the polymer donor PE4 with an extended conjugated π bridge of thieno[3,2-*b*]thiophene, and the polymer showed obviously enhanced crystallinity and charge mobility [29]. Zhou *et al.* synthesized the small molecular donor ZR1 with extended conjugation, which helped to form an optimizing hierarchical morphology and promote charge separation and transport [32].

In this work, we implemented the conjugation expansion strategy to construct polymer donor materials for all-PSCs by utilizing BDT and DTBDT units as the electron-donating monomers. For the electron-withdrawing monomer, the extensively utilized electron acceptor unit, dithieno[3′,2′:3,4;2′′,3′′:5,6]benzo[1,2-*c*][1,2,5]thiadiazole (DTBt), was also conducted the conjugation expansion strategy to synthesize a novel Qx1 unit. Using two different electron donating units, two new polymer donors, PBDT and PDTBDT, were synthesized with obvious differences in conjugation range. As expected, they showed appropriate absorption and energy levels for organic photovoltaics. After blending with polymer acceptor material PYF-T-*o*, the all-PSC devices based on PDTBDT with a lager conjugation range presented an excellent PCE of 13.38%, while devices with PBDT as donor showed a modest PCE of 9.55%. The elevated J_{SC} and FF of PDTBDT devices comparing with them of PBDT were attributed to higher electron mobility and more suitable film morphology originating from stronger crystallinity. Significantly, devices based on PDTBDT showed extremely excellent stability in the air atmosphere. Overall, the novel polymer PDTBDT is a potential donor material for highly stable all-PSCs, which also demonstrated that the conjugation expansion strategy is a simple but efficient method for constructing outstanding polymer donor materials.

The chemical structures of PBDT, PDTBDT and PYF-T-*o* are shown in Fig. 1a. Synthetic routes toward monomer Qx1 and polymers are shown in Scheme S1 (Supporting information). Detailed synthesis procedure, purification method and characterization can be found in Supporting information. The monomer Qx1 can be easily synthesized through a four-step synthetic route, with a high total yield of over 75%. Polymers PBDT and PDTBDT were obtained *via* classical Stille coupling polymerization reactions with M_n of 60.5 and 61.2 kDa, PDI of 1.3 and 1.4, respectively (Fig. S1 in Supporting information). Both of the two polymers show good solubility in common organic solvents. PBDT and PDTBDT showed good thermal stability with decomposition temperatures (5% weight loss) of 414 °C and 433 °C, respectively, as revealed by TGA (thermogravimetric analysis) measurement (Fig. S2 in Supporting information).

The absorption spectra of the two polymers were measured to investigate the effect of different conjugation regions on the absorption properties of polymers. The UV–vis absorption spectra of two polymers and the used polymer acceptor PTF-T-*o* in films and chloroform solution are shown in Fig. 1b and Fig. S3 (Supporting information), respectively, and the corresponding optical data are listed in Table S1 (Supporting information). Both the two polymers show strong absorption in the wavelength range of 450–600 nm, which complements well with the absorption of PYF-T-*o*. In Fig. 1b and Fig. S3, two donors show faintly red-shifting absorption peaks from solution to film state, indicating strong molecular pre-aggregation behavior in solution [33,34]. Significantly, strong shoulder peaks were detected in the absorption spectra of two polymers, reflecting favorable π-π stacking in the polymer films [35,36]. In addition, PDTBDT exhibits a redshifted absorption range comparing with PBDT, which is because that larger conjugation range enhances intramolecular charge transfer and results in a lower bandgap [37]. The steric hindrance between side thiophene and the adjacent Qx1 unit in PDTBDT is weaker than that of PBDT, which is conducive to intermolecular packing, so the intensity of the shoulder peak of PDTBDT is stronger than that of PBDT. These differences can also be reflected in the temperature-dependent absorption spectra of two polymers in Fig. S4 (Supporting information). As demonstrated in many articles, favorable molecular packing facilitates charge transport in devices [38,39].

The energy levels of three polymers were measured by cyclic voltammetry (CV) tests, and the cyclic voltammogram and the resulting energy level diagrams are shown in Figs. 1c and d. The highest occupied molecular orbital (HOMO) levels of PBDT and PDTBDT were determined to be −5.61 and −5.50 eV, while the lowest unoccupied molecular orbital (LUMO) levels of them were

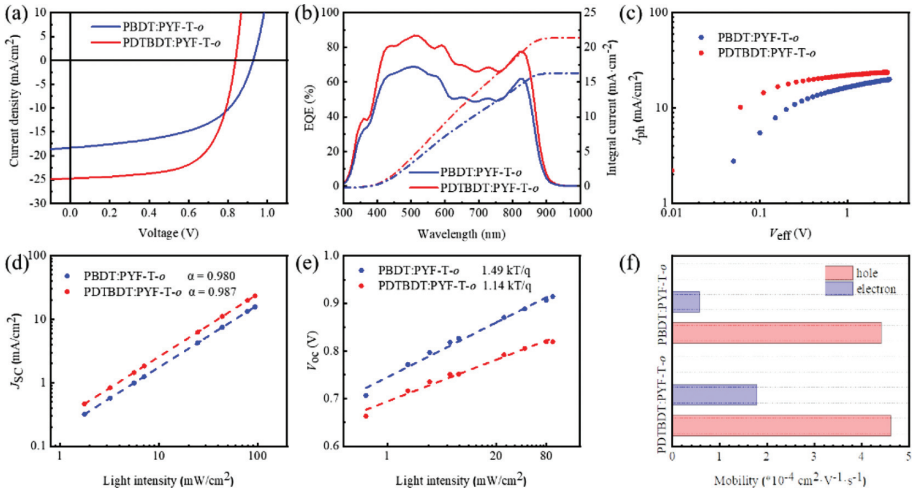

Fig. 2. (a) *J-V* curves, (b) EQE curves, (c) plots of J_{ph} *versus* V_{eff}, (d) dependence of V_{oc} on light intensity, and (e) dependence of J_{sc} on light intensity of the devices based on optimized PBDT:PYF-T-*o* and PDTBDT:PYF-T-*o*. (f) Hole and electron mobility comparison of PBDT:PYF-T-*o* and PDTBDT:PYF-T-*o* blending films.

Table 1
Device parameters and carrier mobilities from SCLC method of the relevant devices. The average values were summarized from 16 parallel devices.

Donor material	V_{OC} (V)	J_{SC} (mA/cm^2)	FF (%)	PCE (%)	μ_h (10^{-4} cm^2 V^{-1} s^{-1})	μ_e (10^{-4} cm^2 V^{-1} s^{-1})	μ_h/μ_e
PBDT	0.93 (0.92±0.01)	18.92 (18.89±0.03)	54.43 (54.39±0.04)	9.55 (9.32±0.23)	4.42	0.58	7.62
PDTBDT	0.84 (0.83±0.01)	24.77 (24.73±0.04)	64.52 (64.50±0.02)	13.38 (13.09±0.29)	4.62	1.79	2.58

calculated to be to be −3.77 and −3.67 eV, respectively. Both the two polymers show perfectly matching energy levels with PYF-T-*o*, proving that they are favorable pairs of the donor and acceptor for OSCs.

A theoretical simulation of two polymers was conducted to demonstrate the effect of different conjugation ranges on molecular backbone conformation and distortion, which is considerable for device active layer morphology and charge transport performance [40,41]. The optimized molecular conformations and frontier molecular orbital levels of two polymers were calculated at the B3LYP/6–31G(d,p) level by the DFT, and the results are shown in Fig. S5 (Supporting information). The dihedral angles of two polymer donor backbone chains were calculated to be 23.22°/12.92°/12.51° and 21.90°/8.04°/8.07°for PBDT and PDTBDT, respectively. As a result, PDTBDT with the larger conjugation range delivers more planar molecular conformation and smaller backbone torsion, which is beneficial for ordered molecular stacking and efficient carrier transport [42]. In addition, the calculated HOMO and LUMO energy level values by DFT were −4.86/−2.54 and −4.83/−2.51 for PBDT and PDTBDT, respectively, which is in agreement with the results from the CV tests.

To further investigate the effect of conjugation ranges in polymer donors on photovoltaic performance, all-polymer solar cell devices employing PBDT or PDTBDT as the donor and PYF-T-*o* as the acceptor were fabricated with a classical device structure of glass/ITO (indium tin oxide)/PEDOT:PSS/active layer/PDINN/Ag. The optimized preparation conditions were spin coating precursor of two polymer donors and PYF-T-*o* in chloroform with the same D/A ratio of 1:1.6 and the same additive of 0.5% CN (1-chloronaphthalene) and concentration of 14 and 12 mg/mL for PBDT and PDTBDT, respectively, without any post-processing. The *J-V* and EQE curves of the resulting devices are shown in Figs. 2a and b and the corresponding photovoltaic parameters are listed in Table 1 for comparison. The PBDT:PYF-T-*o* based devices yielded a modest PCE of 9.55%, with unsatisfactory J_{SC} and FF of 18.92 mA/cm^2 and 54.43%. Replacing BDT unit with DTBDT unit with the larger conjugation range, the PDTBDT:PYF-T-*o* based all-polymer solar cells delivered improved J_{SC} and FF of 24.77 mA/cm^2 and 64.52%, resulting in an outstanding PCE of 13.38%. In addition, the V_{OC}s of PBDT and PDTBDT-based devices are 0.93 and 0.84 V, which is caused by the different HOMO levels of the two polymer donors. Comparing with PBDT, PDTBDT with the larger conjugation range showed planar molecular conformation and stronger molecular crystallinity, resulting in more favorable active layer morphology for charge separation and carrier transport, which facilitates improved J_{SC} and FF.

The EQE curves were measured to verify the short-circuit current obtained in *J-V* test, and the results are shown in Fig. 2b.

Both the two polymers based devices displayed board photon-to-current response in the wavelength range of 300–900 nm, and the PDTBDT-based device showed a stronger photo response signal compared to that of PBDT. This is beneficial for the photo-current conversion and conducive to achieving higher J_{SC}, which is consistent with the tested J_{SC}s of the two devices. In addition, the integrated short-circuit currents ($J_{SC\text{-}cal}$) are 23.54 and 17.98 mA/cm^2 for PDTBDT and PBDT, respectively, which matches the test data within a 5% error.

The exciton dissociation and carrier recombination processes have a critical impact on device performances. The curves of photocurrent density (J_{ph}) *versus* the effective applied voltage (V_{eff}) ware measured to evaluate the exciton dissociation probability (P_{diss}) in two polymers based devices, where J_{ph} is the difference between light current (J_L) and dark current (J_D) and V_{eff} is the difference between the voltage at $J_{ph} = 0$ and the applied voltage. Then, the exciton dissociation probability can be calculated as $J_{ph,0}/J_{sat}$, where $J_{ph,0}$ is the J_{ph} value when the applied voltage is 0 and the J_{sat} is the photocurrent density at a high V_{eff} ($V_{eff} = 2$ V in this case) [43,44]. As shown in Fig. 2c, the resulting P_{diss} of PBDT and PDTBDT based devices are 87.8% and 93.6%, respectively, indicating that the extended conjugation range and enhanced

crystallinity of polymer donor can facilitate efficient exciton dissociation in the D/A interface and lead to higher J_{SC} and FF. The charge recombination kinetics in two devices was also explored by measuring the J_{SC} and V_{OC} under different light intensity (P_{light}). J_{SC} and P_{light} can be fitted as the formula of $J_{SC} \propto P_{light}^{\alpha}$, where α is the exponential factor that can indicate the degree of bimolecular recombination. The closer α is to 1, the lower the possibility of bimolecular recombination [45,46]. As shown in Fig. 2d, the α values of PBDT and PDTBDT-based devices was determined to be 0.980 and 0.987, respectively, demonstrating a lower degree of bimolecular recombination in PDTBDT-based device. Then, based on the proportional relationship between V_{OC} and logarithm of P_{light} ($V_{OC} \propto \ln P_{light}$), the V_{OC}-lnP_{light} curve was prepared, and the slope of the fitted line was used to reflect the extent of trap-assisted recombination in devices. It is widely considered that the more the slope deviates from $1kT/q$ (k is Boltzmann's constant, T is temperature, and q is the elementary charge), the greater the degree of trap-assisted recombination [47,48]. As shown in Fig. 2e, the slopes of PDTBDT and PBDT-based devices were $1.14kT/q$ and $1.49kT/q$, suggesting relatively less trap-assisted recombination in PDTBDT-based devices. In general, devices with PDTBDT as the donor showed higher exciton dissociation probability and lower carrier recombination probability, resulting in higher J_{SC} and FF compared with that of PBDT.

The electron and hole mobilities (μ_e and μ_h) of the two polymer donors were also tested to compare their carrier transport properties using the space charge limited current (SCLC) methods. The employed device structures for electron and hole mobilities are ITO/ZnO/active layer/PDINN/Ag and ITO/PEDOT:PSS/active layer/MoO_3/Ag and the results are summarized in Fig. 2f and Fig. S6 (Supporting information), Table 1 and Table S3 (Supporting information). For neat films, PDTBDT showed a higher μ_h of 9.10×10^{-4} cm^2 V^{-1} s^{-1} compared with that of PBDT of 6.34×10^{-4} cm^2 V^{-1} s^{-1}. After blending with PYF-T-*o*, the μ_e and μ_h of devices are $1.79 \times 10^{-4}/4.62 \times 10^{-4}$ and $0.58 \times 10^{-4}/4.42 \times 10^{-4}$ with the relevant μ_h/μ_e values of 2.58 and 7.62 for PDTBDT and PBDT, respectively. Obviously, PDTBDT with lager conjugation range shows more favorable and balanced charge transport properties compared with PBDT, which is significant to achieve outstanding J_{SC} and FF. This also demonstrates that conjugation expansion strategy can be used to construct organic semiconductor materials suitable for exciton dissociation and carrier transport.

Atomic force microscopy (AFM) and transmission electron microscopy (TEM) measurements were carried out to further investigate the film morphology of the blend films. As shown in Fig. 3, both two polymers-based blending films showed proper morphology for carrier transportation. Significantly, the TEM image of PDTBDT-based blending film exhibited a clear fiber-like structure, implying strong molecular stacking. In the AFM images, PDTBDT-based blend film showed a smoother surface with a root-mean-square roughness (R_q) of 0.85 nm, which could induce better contact between the active layer and the adjacent interlayer, leading to improved carrier transport properties and higher FF. These results demonstrated that the strong crystallinity sourced from larger conjugation range of the polymer donor can induce the formation of an excellent film morphology that is more favorable for carrier transport, resulting in significantly improvement of J_{SC} and FF.

Molecular stacking and orientation have a crucial impact on the performance of organic semiconductor devices. The grazing incidence wide angle X-ray scattering (GIWAXS) measurements were performed to gain a deeper understanding of molecules packing in films. As shown in Figs. 3g-i and Fig. S7 (Supporting information), both two polymers based neat and blending films showed a predominant molecular stacking model of face-on orientation, which guarantees the carrier transport properties in the vertical direction

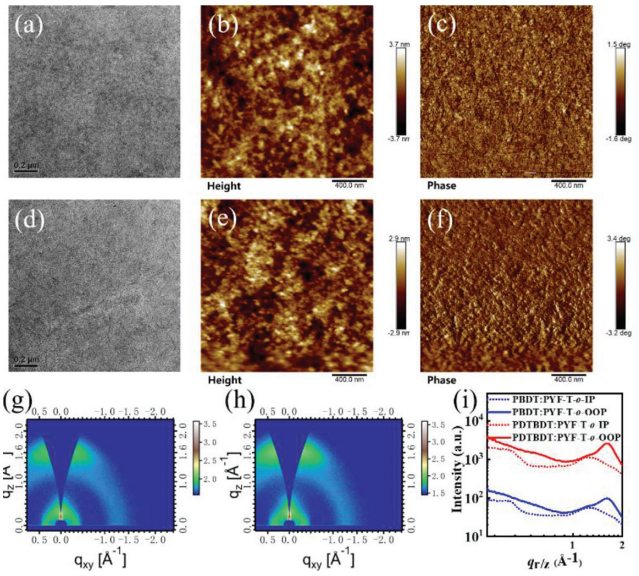

Fig. 3. TEM images of (a) PBDT:PYF-T-*o* and (d) PDTBDT:PYF-T-*o* blend films. AFM height images of (b) PBDT:PYF-T-*o* and (e) PDTBDT:PYF-T-*o* blend films. AFM phase images of (c) PBDT:PYF-T-*o* and (f) PDTBDT:PYF-T-*o* blend films. 2D GIWAXS patterns of (g) PBDT:PYF-T-*o* and (h) PDTBDT:PYF-T-*o* blend films. (i) The OOP and IP curves of PBDT:PYF-T-*o* and PDTBDT:PYF-T-*o* blend films.

in the films. PDTBDT and PBDT based neat films delivered a similar π–π stacking (010) peaks at $q_z = 1.62$ Å^{-1} (d-spacing = 3.88 Å) and $q_z = 1.63$ Å^{-1} (d-spacing = 3.85 Å) along the out-of-plane (OOP) directions, respectively (Table S2 in Supporting information), indicating similar molecular packing properties with ordered face-on orientation and tight polymer chain packing. Furthermore, the crystalline coherence lengths (CCLs) of the (010) peaks in the OOP direction of PBDT and PDTBDT based blending films were calculated to be 16.49 and 20.71 Å (Table S2), implying that PDTBDT has a stronger crystallinity compared with PBDT in blend films. These observations demonstrated that the extended conjugation range in PDTBDT helps it to form better crystallization and film morphology in the blending film, which promotes carrier transport mobility.

Excellent long-term stability is one of the outstanding advantages of all-polymer solar cells. To investigate the effect of the conjugation expansion strategy on the stability of solar cell devices based on two polymers, we measured the long-term stability of unencapsulated devices in air and nitrogen atmospheres. The test results are shown in Figs. 4a and b. As expected, the storage stability of the device in the nitrogen atmosphere is much better than that in the air atmosphere. Both devices based on two polymers exhibited over 85% of initial efficiency after 500 h in N_2 glove box, while over 65% of beginning efficiency PCE were detected in the air atmosphere devices after the same time. Afterwards, PDTBDT-based devices showed higher efficiency retention than PBDT ones, demonstrating better long-term stability. This may be due to the strong crystallinity of PDTBDT, which makes its blend film denser and effectively resist the erosion of water and oxygen under air conditions [49,50]. These results strongly prove that the conjugate expansion strategy is indeed beneficial to obtain all polymer solar cell devices with excellent long-term stability.

To gain a deeper understanding of the effect of air conditions on the device, we conducted TEM measurements of the blending films placed in N_2 and air for 500 h, and the results are shown in Figs. 4c-j. It can be noted that blending films based on both polymers showed very small changes in morphology after being stored in N_2 for 500 h. However, the air atmosphere samples exhibited obvious differences after 500 h. The blend film of PDTBDT:PYF-T-*o* still exhibited a similar network structure with a clear interface

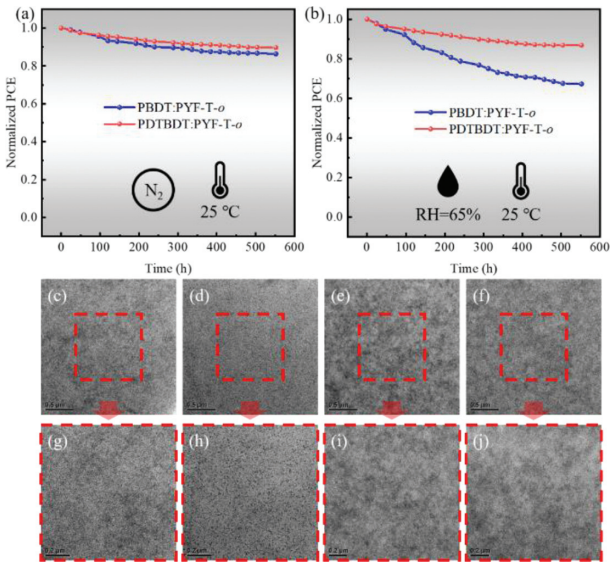

Fig. 4. Stability of all-polymer solar cell devices based on (a) PBDT:PYF-T-*o* and (b) PDTBDT:PYF-T-*o* in N_2 and air atmosphere. TEM images with different magnification of blending films placed in N_2 and air for 500 h. (c, g) PBDT:PYF-T-*o* in N_2; (d, h) PBDT:PYF-T-*o* in air; (e, i) PDTBDT:PYF-T-*o* in N_2; (f, j) PDTBDT:PYF-T-*o* in air.

between the donor and acceptor domains, while the PBDT:PYF-T-*o* ones showed very inappropriate morphology, which is not conducive to the efficient transport of carriers. In general, the blending films of PDTBDT show better resistance to water and oxygen in the air atmosphere, and thus the devices based on it obtain better stability.

In summary, two novel π-conjugated polymer donors PBDT and PDTBDT with different conjugation range were designed and synthesized to explore the effect of the conjugation expansion strategy on all polymer solar cell device efficiency and stability. Comparing with PBDT, PDTBDT with a lager conjugation range showed greater aggregation properties and more favorable molecular packing. After blending with PYF-T-*o*, the corresponding all-PSCs delivered higher J_{SC} and FF than the PBDT-based devices, resulting in an outstanding PCE of 13.38%, while devices based on PBDT:PYF-T-*o* showed a modest PCE of 9.55%. Further characterization demonstrated that the PDTBDT:PYF-T-*o* based devices displayed higher exciton dissociation probability, lower carrier recombination probability, more balanced charge transport properties, and more favorable film morphology. Moreover, the PDTBDT:PYF-T-*o* devices retain 0.86 of the initial PCE after over 500 h in the air atmosphere, exhibiting significantly improved stability. These results indicate that the conjugation expansion strategy is simple but efficient for obtaining efficient and stable all-PSCs. We believe that the conjugation expansion strategy is a promising route for the future application of all-PSCs in large-scale commercialization.

Declaration of competing interest

The authors declare no competing financial interest.

Acknowledgments

We acknowledge financial support provided by the National Natural Science Foundation of China (Nos. 21822503 and 51973043), and the and the CAS-CSIRO Joint Project of Chinese Academy of Sciences (No. 121E32KYSB20190021).

Supplementary materials

Supplementary material associated with this article can be found, in the online version, at doi:10.1016/j.cclet.2022.108019.

References

[1] A.J. Heeger, Adv. Mater. 26 (2014) 10–28.
[2] O. Inganas, Adv. Mater. 30 (2018) 1800388.
[3] G. Li, R. Zhu, Y. Yang, Nat. Photonics 6 (2012) 153–161.
[4] Z. Zheng, J. Wang, P. Bi, et al., Joule 6 (2022) 171–184.
[5] J. Liu, P. Jiang, Y. Wang, et al., Chin. Chem. Lett. 31 (2020) 119–124.
[6] Z. Liu, C. Bao, G. Zhang, et al., Chin. Chem. Lett. 31 (2020) 2459–2464.
[7] L. Shao, F. Tong, M. Zhu, et al., Chin. Chem. Lett. 31 (2020) 2452–2458.
[8] Y. Zhao, L. Zhou, X. Wu, et al., Chin. Chem. Lett. 32 (2021) 1359–1362.
[9] Q. Burlingame, M. Ball, Y.L. Loo, Nat. Energy 5 (2020) 947–949.
[10] L. Duan, A. Uddin, Adv. Sci. 7 (2020) 1903259.
[11] M. Jorgensen, K. Norrman, S.A. Gevorgyan, et al., Adv. Mater. 24 (2012) 580–612.
[12] Y. Kong, Y. Li, J. Yuan, et al., InfoMat 4 (2022) e12271.
[13] H. Yu, Y. Wang, H.K. Kim, et al., Adv. Mater. 34 (2022) 2200361.
[14] D. Zhou, C. Liao, S. Peng, et al., Adv. Sci. 9 (2022) 2202022.
[15] T. Kim, J.H. Kim, T.E. Kang, et al., Nat. Commun. 6 (2015) 8547.
[16] X. Liu, C. Zhang, C. Duan, et al., J. Am. Chem. Soc. 140 (2018) 8934–8943.
[17] B. Fan, P. Zhu, J. Xin, et al., Adv. Energy Mater. 8 (2018) 1703085.
[18] Y. Guo, Y. Li, O. Awartani, et al., Adv. Mater. 29 (2017) 1700309.
[19] Q. Fan, H. Fu, Q. Wu, et al., Angew. Chem. Int. Ed. 60 (2021) 15935–15943.
[20] Z.G. Zhang, Y. Yang, J. Yao, et al., Angew. Chem. Int. Ed. 56 (2017) 13503–13507.
[21] Q. Yang, W. Yu, J. Lv, et al., Dyes Pigm. 200 (2022) 110180.
[22] Z. Li, F. Peng, H. Quan, et al., Chem. Eng. J. 430 (2022) 132711.
[23] D. Chen, S. Liu, B. Huang, et al., Small 18 (2022) 2200734.
[24] W. Xu, X. Zhu, X. Ma, et al., J. Mater. Chem. A 10 (2022) 13492–13499.
[25] F. Peng, K. An, W. Zhong, et al., ACS Energy Lett. 5 (2020) 3702–3707.
[26] J. Zhang, C.H. Tan, K. Zhang, et al., Adv. Energy Mater. 11 (2021) 2102559.
[27] S.H. Kang, D. Lee, W. Choi, et al., Macromolecules 55 (2022) 4367–4377.
[28] Z. Jiang, H. Li, Z. Wang, et al., Macromol. Rapid Commun. 39 (2018) 1700872.
[29] A. Tang, Q. Zhang, M. Du, et al., Macromolecules 52 (2019) 6227–6233.
[30] J.H. Kim, J.B. Park, F. Xu, et al., Energy Environ. Sci. 7 (2014) 4118–4131.
[31] L. Huo, T. Liu, X. Sun, et al., Adv. Mater. 27 (2015) 2938–2944.
[32] R. Zhou, Z. Jiang, C. Yang, et al., Nat. Commun. 10 (2019) 5393.
[33] D. Meng, H. Fu, C. Xiao, et al., J. Am. Chem. Soc. 138 (2016) 10184–10190.
[34] L. Xue, Y. Yang, J. Xu, et al., Adv. Mater. 29 (2017) 1703344.
[35] S. Li, L. Ye, W. Zhao, et al., Adv. Mater. 28 (2016) 9423–9429.
[36] Y. Lin, F. Zhao, S.K.K. Prasad, et al., Adv. Mater. 30 (2018) 1706363.
[37] J. Liu, S. Chen, D. Qian, et al., Nat. Energy 1 (2016) 16089.
[38] B. Fan, K. Zhang, X.F. Jiang, et al., Adv. Mater. 29 (2017) 1606396.
[39] Y. Chen, Y. Geng, A. Tang, et al., Chem. Commun. 55 (2019) 6708–6710.
[40] S. Mamba, D.S. Perry, M. Tsige, et al., J. Phys. Chem. A 125 (2021) 10593–10603.
[41] M. Li, M. Zeng, X. Tang, et al., ACS App. Energy Mater. 4 (2021) 8117–8129.
[42] M. Jiang, H.-r. Bai, H.-f. Zhi, et al., ACS Energy Lett. 6 (2021) 2898–2906.
[43] K. Yang, J. Wang, Z. Zhao, et al., Chem. Eng. J. 435 (2022) 134973.
[44] M. Nam, J. Na, J. Shin, et al., Nano Energy 74 (2020) 104883.
[45] C. Xu, Z. Zhao, K. Yang, et al., J. Mater. Chem. A 10 (2022) 6291–6329.
[46] H. Chen, T. Zhao, L. Li, et al., Adv. Mater. 33 (2021) 2102778.
[47] V.V. Brus, Org. Electron. 29 (2016) 1–6.
[48] V.V. Brus, C.M. Proctor, N.A. Ran, et al., Adv. Energy Mater. 6 (2016) 1502250.
[49] H. Bronstein, Z. Chen, R.S. Ashraf, et al., J. Am. Chem. Soc. 10 (2011) 3272–3275.
[50] J.W. Ha, C.E. Song, H.S. Kim, et al., ACS Appl. Mater. Interfaces 46 (2020) 51699–51708.